Title
Adjoint-Based Inversion of Geodetic Data for Sources of Deformation and Strain

Journal
Journal of Geophysical Research: Solid Earth, 126(9)

ISSN
2169-9313

Authors
Smith, J Torquil
Vasco, DW

Publication Date
2021-09-01

DOI
10.1029/2021jb021735

Peer reviewed

Adjoint-based inversion of geodetic data for sources of deformation and strain

J. Torquil Smith [1] **and D. W. Vasco** [1]

[1]Energy Geosciences Division, Lawrence Berkeley National Laboratory, Berkeley, California.

Key Points:

- An adjoint-based gradient calculation provides the basis for an efficient inversion approach, using observations of quasi-static deformation to infer a distribution of source parameters, such as aquifer volume change or fault/fracture aperture changes.
- A comparison with a conventional sensitivity-based inversion technique demonstrates the accuracy of the adjoint-based gradients and the efficiency of the approach in finding a solution to the inverse problem.
- An application to Interferometric Synthetic Aperture Radar line-of-sight displacement data from the Tulare Basin in California's Central Valley indicates that it is possible to satisfy the observations with a model containing aquifer volume changes near documented well locations.

Corresponding author: D. W. Vasco, `dwvasco@lbl.gov`

Abstract

An adjoint-based formulation leads to a particularly efficient approach for inverting geodetic measurements for the source of the deformation. Specifically, the quantities necessary to iteratively improve the fit to the observations can be computed with just three forward calculations, one to obtain the current residuals, another to solve the adjoint problem, and a third to compute the step length. An inversion algorithm utilizing the adjoint-based gradient is applied to a set of Interferometric Synthetic Aperture Radar (InSAR) data gathered between 2016 and 2018 over the Tulare Basin in California's Central Valley. Because the measured deformation is due to groundwater withdrawal, a penalty function is included in the inversion to avoid placing aquifer volume change in locations that are far from any documented wells. The solution of the inverse problem provides estimates of aquifer compaction that provide a match to the observed range changes while honoring the well data. The solution indicates an average aquifer volume loss of 2.17 km^3/year over the two year period from January 2016 to January 2018, encompassing one drought year (2016) and one wet year (2017). This magnitude of lost volume is compatible with the 3.1 km^3/year decrease in water volume for the entire Central Valley, estimated from GRACE satellite gravity data.

Plain Language Summary

A new approach allows for the inversion of quasi-static deformation data for parameters describing the source, such as aquifer/reservoir volume changes or fracture aperture changes. The technique utilizes the solution of the adjoint problem to find the model parameter gradients necessary for an iterative update of an initial model. Each update of the source model requires the equivalent of three forward simulations, one to determine the residuals, one to solve the adjoint problem, and one the determine the step length. The technique is applied to InSAR line-of-sight displacement data from California's Central Valley in order to estimate aquifer volume loss in the Tulare Basin.

1 Introduction

With the increasing use of large-scale data sets, as generated by satellite-based observations from Interferometric Synthetic Aperture Radar (InSAR) (Galloway et al., 1998; Ferretti, 2014), the Gravity Recovery and Climate Experiment (GRACE) (Liu et al., 2019), and even by the seismic time-strains that are detected during reservoir monitoring (Hatchell & Bourne, 2005; Hodgson et al., 2007), the modeling of quasi-static deformation is becoming an ever larger computational challenge. Furthermore, given the larger areas of the Earth that are often under study, the three-dimensional nature of the structural features in many of todays geologic models cannot be ignored. The sources of quasi-static deformation are often widely distributed, as in the case of subsidence driven by large-scale groundwater extraction from thousands of wells (Vasco et al., 2019), and for deformation due to hydrothermal/volcanic activity in large systems containing faults and fractures, such as the Yellowstone Caldera (Chang et al., 2007). Thus, the representation of the often three-dimensional source can require thousands of parameters, leading to a very large inverse problem for the distributed source.

Large-scale three-dimensional numerical simulations of quasi-static displacements, in a fully heterogeneous medium, can take several hours of computation for current finite-difference or finite element codes. This can lead to computational difficulties when inverting large data sets using sensitivity-based or stochastic approaches. Boundary element methods may provide much needed efficiency (Gwinner & Stephan, 2018), but we are not aware of any published large-scale inversions for a fully three-dimensional, heterogeneous medium. As shown below, even our implicit finite-difference code, which takes roughly 3 minutes for a simulation of displacements in an elastic medium described by

over 1 million nodes, requires roughly 230 hours to solve for volume changes at all 4900 source grid blocks describing the source. Techniques utilizing adjoints to estimate gradients for an iterative conjugate gradient algorithm provide an efficient approach for large-scale inversions (Plessix, 2006). Such approaches have a long history in the geosciences, dating from their early use in fluid flow and pressure inversion (Jacquard & Jain, 1965). However, their use in the analysis of quasi-static deformation had been restricted to the more difficult inverse problem associated with the characterization of the medium properties, such as poroelastic moduli and the flow properties (Iglesias & McLaughlin, 2012; Hesse & Stadler, 2014). Though this approach is more comprehensive, it is nonlinear and requires modeling the fully coupled deformation and flow within the complex source region. The use of adjoints for the much simpler source identification problem, which solves for an equivalent source, had been restricted to the dynamic case associated with the propagation of elastic waves (Kaderli et al., 2018). Recently, a Green's function formulation of an adjoint-based inverse problem for the source of quasi-static deformation was published (Vasco & Mali, 2021). In that work, the application of the Green's function to the distribution of sources was approximated by a numerical simulator.

Here, we dispense with the Green's functions entirely, and formulate the adjoint-based inverse problem directly in terms of the governing equations that are utilized by the numerical simulator. This results in an extremely efficient approach for estimating a distribution of sources of quasi-static deformation. Each gradient calculation only requires two solutions of the forward problem, one to compute the residuals, and an adjoint solution whereby the current residual surface displacements are applied as sources of deformation. The gradient components are given by the resulting source grid block volume changes. The technique is applied to Interferometric Synthetic Aperture Radar (InSAR) data from California's Central Valley (Figure 1) in order to estimate aquifer compaction due to groundwater pumping. In this area InSAR data has been used to improve our understanding of the hydrodynamics of the groundwater aquifers and their seasonal variations (Murray & Lohman, 2018; Neely et al., 2020; Vasco et al., 2019). The approach can be used for other investigations, such as the study of ground deformation due to oil production, as observed to the south of our area of interest (Fielding et al., 1998; Vasco et al., 2017), and the study of coseismic and post-seismic slip associated with faulting (Moore et al., 2017).

2 Methodology

Our goal is to use measured displacements or strains to define a distributed source model that generates the observed deformation. The source could be variable volume change within an aquifer/reservoir or spatially-varying aperture/shear on a fault plane (Vasco et al., 2010). The forward problem relates the changes in the source strength, denoted by $\mathbf{m}$ to the deformation at the surface, $\mathbf{u}$ or, more generally, outside of the reservoir or aquifer. The governing equations are in the form of a system of linear partial differential equations. For a numerical solution one typically writes these equations as a discrete linear system

$$\mathbf{A}\mathbf{u} = \mathbf{B}\mathbf{m} + \mathbf{b} \tag{1}$$

that may be formulated and solved using methods such as finite differences (Phillips & Rose, 1986; Hattel & Hansen, 1995). Given a set of boundary conditions and source functions $\mathbf{m}$, we can solve these equations for the three components of the displacement vector $\mathbf{u}$ in the finite-difference mesh. Thus, $\mathbf{u}$ will contain 3 times the number of nodes, say M, in the finite-difference mesh. The matrix $\mathbf{B}$ maps the source magnitudes into the nodes of the finite-difference mesh. For example, if the sources are N_g grid blocks encompassing many nodes of the underlying finite-difference mesh, then $\mathbf{B}$ is a map from the grid block to all of the associated nodes. Thus, the matrix $\mathbf{B}$ have dimensions of $3\times M$ by N_g for this finite-difference example. The forward problem involves determining the displacements in the medium given a set of source functions $\mathbf{m}$, and, if present, a set

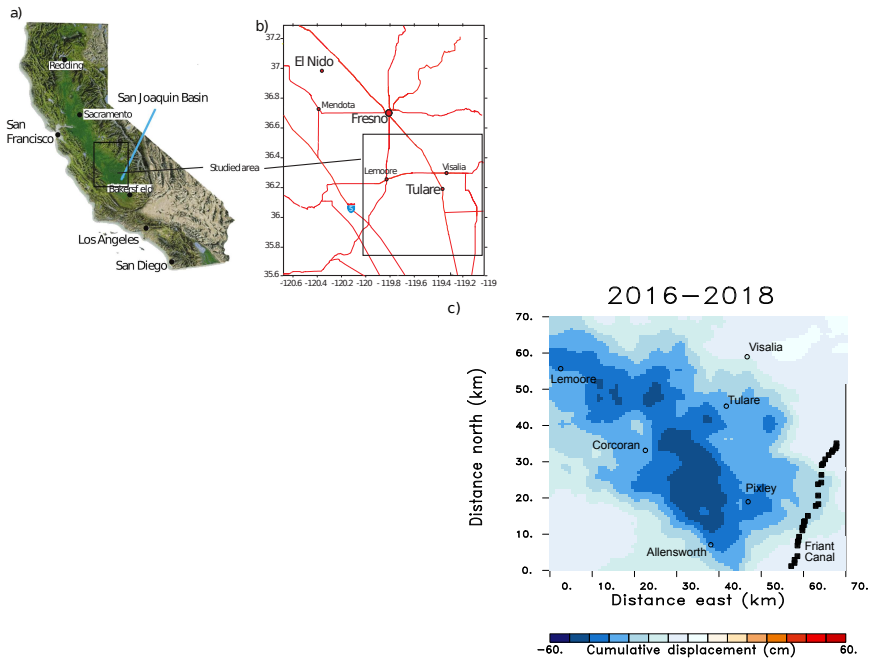

Figure 1. (a) Location of the area within California's Central Valley, (b) Schematic map of the region around the study area, (c) Interferometric Synthetic Aperture Radar range change observations associated with groundwater withdrawal from aquifers in the Tulare Basin of the Central Valley in California. The curve of filled black squares denotes the location of the Friant canal.

of body forces $\mathbf{b}$. The inverse problem involves determining $\mathbf{m}$ from a set of observed displacements or, as shown next, a linear function of observed displacements. In order to determine $\mathbf{m}$ in terms of the subset of $\mathbf{u}$ that correspond to measured one must reformulate the linear system (1) due to the presence of the intermediate displacements, those components of $\mathbf{u}$ that do not correspond to observed quantities. Thus, one does not solve equation (1) directly for $\mathbf{m}$, as this is an under-constrained problem. Typically, one resorts to a Green's function formulation in order to write the observed displacements directly in terms of the source parameters $\mathbf{m}$, effectively solving the forward problem (1) for $\mathbf{m}$ (Menke, 2018; Vasco & Mali, 2021). We avoid the use of Green's functions, due to the difficulty of computing them for complicated three-dimesional variations in elastic properties, and solve the inverse problem for $\mathbf{m}$ directly in terms of a numerical simulation, that is, a numerical solution of the forward problem (1). Thus, we show how to construct an iterative model update with three simulations, first with a current model to calculate the residuals, then with the residual displacements as sources at the observation points, the adjoint problem, and lastly to compute the step length or magnitude of the update.

The observed deformation, may be some linear function of the displacements, such as tilt, range change from Interferometric Synthetic Aperture Radar (InSAR), or time strains from three-dimensional seismic data. This transformation from the full displacement vector to the observed components of deformation can be written as

$$\mathbf{d} = \mathbf{C}\mathbf{u} + \mathbf{e}. \tag{2}$$

where $\mathbf{C}$ is the linear mapping that may represent projections in the case of InSAR observations, or spatial differentiations in the case of tilt and strain. The matrix $\mathbf{C}$ has a

strong influence on the resolution provided by the geodetic data. For example, in the case of seismic time strains, the matrix has many more non-zero elements relating the displacements within the entire volume under study to the seismic observations. For geodetic data gathered as the Earth's surface many of the displacements in $\mathbf{u}$ are projected to zero, leading to poor depth resolution. The vector $\mathbf{e}$ denotes the data residuals, the observed minus the calculated line-of-sight displacements. For the inverse problems we seek a solution that minimizes the misfit or the residual vector given by

$$\mathbf{e} = \mathbf{d} - \mathbf{C}\mathbf{u}. \tag{3}$$

The inverse problem is typically unstable due to issues related to the uniqueness or resolution, particularly for observations obtained at the Earth's surface. A common approach to mitigate the uniqueness issue and to stabilize the inverse problem is to introduce a regularization penalty term (Menke, 2018). Some examples of such penalty terms are the model roughness, the deviation of the model from some desired or a priori model, the weighted model parameters with weights that increase away from a particular set of locations (Vasco et al., 2019). One can generally write the penalty term in the form of a quadratic function of the model parameters

$$P(\mathbf{m}) = (\mathbf{r} - \mathbf{R}\mathbf{m})^t (\mathbf{r} - \mathbf{R}\mathbf{m}). \tag{4}$$

An objective function consisting of a linear combination of the data misfit and the regularization term

$$J(\mathbf{m}) = \mathbf{e}^t\mathbf{e} + \lambda (\mathbf{r} - \mathbf{R}\mathbf{m})^t (\mathbf{r} - \mathbf{R}\mathbf{m}) \tag{5}$$

where λ is a scalar specifying the relative importance of the penalty term. The inverse problem entails minimizing the quadratic (5), perhaps subject to inequality constraints. There are several methods for accomplishing this minimization including stochastic and iterative approaches. Here, we will operate under the assumption that the forward problem is computationally intensive and may take hours or days for a complete solution. Thus, stochastic approaches that can require thousands of forward simulations for large problems are usually not feasible. Even iterative techniques may not be practical unless they are extremely efficient.

The critical step for many iterative methods is the computation of the gradient of the misfit function $J(\mathbf{m})$ with respect to the model parameters $\mathbf{m}$. For example, in the application below we describe the conjugate gradient algorithm for minimizing a penalized misfit function defining the inverse problem. The simplest and most direct method for computing the gradient, is a perturbation approach in which each model parameter is subject to a small deviation and a forward simulation is conducted to estimate the change in the observations. This scheme requires $N+1$ simulations where N is the number of model parameters and is impractical for large models with thousands of parameters. As noted in the Introduction, we describe an alternative approach that is based upon the solution of the adjoint problem. We can formulate the method using equations (1) and (3) to write $\mathbf{e}$ as

$$\mathbf{e} = \mathbf{d} - \mathbf{C}\mathbf{A}^{-1} (\mathbf{B}\mathbf{m} + \mathbf{b}). \tag{6}$$

Substituting this into equation (5) gives

$$J(\mathbf{m}) = \left[\mathbf{d} - \mathbf{C}\mathbf{A}^{-1} (\mathbf{B}\mathbf{m} + \mathbf{b})\right]^t \left[\mathbf{d} - \mathbf{C}\mathbf{A}^{-1} (\mathbf{B}\mathbf{m} + \mathbf{b})\right] \tag{7}$$

$$+\lambda (\mathbf{r} - \mathbf{R}\mathbf{m})^t (\mathbf{r} - \mathbf{R}\mathbf{m}),$$

an expression for the penalized misfit functional in terms of the source parameters $\mathbf{m}$. Direct differentiation provides an expression for the gradient with respect to the source parameters

$$\nabla_m J(\mathbf{m}_i) = -2\mathbf{B}^t \left(\mathbf{A}^t\right)^{-1} \mathbf{C}^t [\mathbf{d} - \mathbf{C}\mathbf{u}_i] - 2\lambda \mathbf{R}^t (\mathbf{r} - \mathbf{R}\mathbf{m}_i). \tag{8}$$

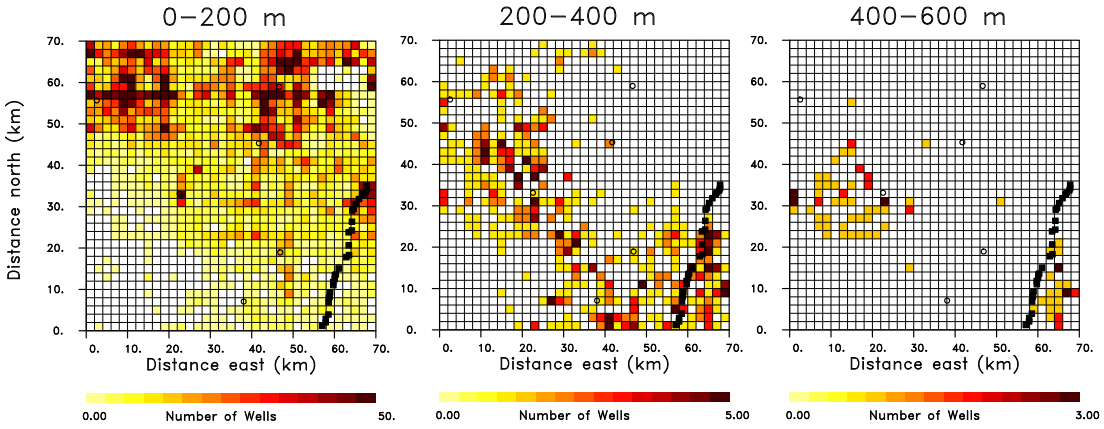

Figure 2. Well densities (number of wells/grid block) for the upper three depth ranges in the model. The densities were used to compute the distance weighting in the matrix $\mathbf{D}$ is the penalized misfit function (12). The open circles denote the locations of the towns labeled in Figure 1. The filled squares denote the path of the Friant canal.

An algorithm for $\nabla_m J$ can be executed in two main steps. The first step involves solving the forward problem (1) for the displacement components $\mathbf{u}_i$, given an initial or current source model $\mathbf{m}_i$ where we consider the i-th iteration of the iterative algorithm, and computing the residuals $\mathbf{e}_i = \mathbf{d} - \mathbf{C}\mathbf{u}_i$. The second step is to solve the companion problem

$$\mathbf{A}^t \mathbf{w}_i = \mathbf{C}^t \left(\mathbf{d} - \mathbf{C}\mathbf{u}_i \right) \tag{9}$$

or

$$\mathbf{A}^t \mathbf{w}_i = \mathbf{C}^t \mathbf{e}_i \tag{10}$$

for $\mathbf{w}_i$. Equation (10) can be solved numerically if the coefficients composing the matrix $\mathbf{A}$ are available. However, many geomechanical simulators form the coefficient matrix $\mathbf{A}$ internally or use numerical methods such as finite-elements or finite-volume to solve the forward problem as encapsulated in equation (1). We will assume that such a simulator is available for solving the forward problem associated with the simulation of deformation. Note that the problem (10) is the adjoint problem, which for a linear operator is given by $(\mathbf{y}, \mathbf{A}\mathbf{x}) = (\mathbf{A}^*\mathbf{y}, \mathbf{x})$ where $\mathbf{x}$ and $\mathbf{y}$ are two vectors and the brackets denote the inner product of two vectors. For a matrix operator $\mathbf{A}^* = \mathbf{A}^t$, and the adjoint is equivalent to the transpose of the matrix (Stakgold, 1979). If the forward problem is self-adjoint then $\mathbf{A}^* = \mathbf{A}^t = \mathbf{A}$, e.g. the governing equations for elastic deformation, formulated in terms of displacements, then equation (10) is simply the forward problem with the residuals as source terms. The final expression for the gradient is

$$\nabla_m J(\mathbf{m}_i) = -2\mathbf{B}^t \mathbf{w}_i - 2\lambda \mathbf{R}^t \left(\mathbf{r} - \mathbf{R}\mathbf{m}_i \right), \tag{11}$$

and it is obtained with the equivalent of two solutions of the forward problem, similar to adjoint approaches for estimating gradients in order to solve inverse problems. Specifically, given an initial source at the i-th iteration, one solves the forward problem (1) for the residuals $\mathbf{e}_i$, and then the adjoint problem (10) for $\mathbf{w}_i$, where the residuals are used as sources of deformation. As shown below, the gradient can be incorporated into the conjugate gradient algorithm or the variable metric method (Press et al., 1992; Fletcher, 2000) for the minimization of the penalized misfit function $J(\mathbf{m})$ given by expression (5).

3 Application to subsidence in California's Central Valley

Over-subscribed groundwater basins and their sustainability is a world-wide issue that is exacerbated by advancing climate change. In order to better understand the po-

tential lifetime of groundwater resources one needs to understand the existing volume of water, the recharge of the system, and the rate of withdrawal. Unfortunately, many jurisdictions lack the data needed to accurately determine these important quantities. For example, in California individual well usage is not currently reported to any authority or governing agency, though this may change in the future. Therefore, it is necessary to estimate extracted water volumes by other means, such as the correlation of electrical usage with pumping rates. Surface subsidence in major basins, such as in the Central Valley of California (Figure 1), has been linked to aquifer compaction and groundwater pumping (Faunt et al., 2010; Galloway et al., 1998). Detailed and quantitative estimates of surface subsidence are provided by the Sentinel-1a/b synthetic aperture radar (SAR) data (Farr & Liu, 2015) that are freely available from the European Space Agency, providing repeat coverage every 6 to 12 days. As noted in the Appendix, our line-of-sight displacement data may be downloaded from the Zenodo repository. The satellite heading is 348^o and the look angle is 39^o from vertical, so that the line-of-sight displacement is somewhat more sensitive to vertical displacements. Data were provided to us by NASA's Jet Propulsion Laboratory (JPL), processed using the Interferometric Scientific Computing Environment (ISCE) which implements the Small Baseline Subset (SBAS) approach (Farr & Liu, 2015; Vasco et al., 2019). Such subsidence can be mapped into aquifer volume changes and provides a lower bound on changes in water volume (Vasco et al., 2019). In order to accurately localize these estimates, the volume changes need to be tied to known wells. Fortunately, there exists a database of wells that may be used in this regard. The characteristics of all wells that have been drilled and completed must be sent to the state of California, providing their location and depth of penetration. As an example we plot the well density (number of wells/grid block) for the top three layers of our model in Figure 2. Using this information, it is possible to define a quadratic penalty function of the form (4) to bias the solution set to locate volume change in the vicinity of documented wells (Vasco et al., 2019). In particular, we seek to minimize the penalized misfit function

$$J(\mathbf{m}) = \mathbf{e}^t\mathbf{e} + \lambda \mathbf{m}^t\mathbf{D}\mathbf{m} \tag{12}$$

where $\mathbf{D}$ is a matrix with diagonal entries that are proportional to the distance from the corresponding grid block to the location of the nearest well. The residuals are given by $\mathbf{e}$ in equation (2) where, for this application, the matrix $\mathbf{C}$ takes the form of a projection of the displacement vector for each surface node onto the look vector $\mathbf{l}$ for the Sentinel satellite.

The conjugate gradient algorithm provides an iterative approach for minimizing the quadratic penalized misfit function $J(\mathbf{m})$ (Fletcher, 2000) and allows us to find a distribution of aquifer volume change that minimizes the misfit to the observations with a model that has aquifer compaction near known wells. Specifically, for a given model from the i-th iteration, the algorithm provides an update of the form

$$\mathbf{m}_{i+1} = \mathbf{m}_i + \alpha_i \mathbf{h}_i, \tag{13}$$

where, for $i = 0$,

$$\mathbf{h}_0 = -\nabla J(\mathbf{m}_0), \tag{14}$$

otherwise,

$$\mathbf{h}_i = \gamma \mathbf{h}_{i-1} - \nabla J(\mathbf{m}_i), \tag{15}$$

with

$$\gamma = |\nabla J(\mathbf{m}_i)|^2 / |\nabla J(\mathbf{m}_{i-1})|^2, \tag{16}$$

[e.g., (Press et al., 1992)]. This algorithm is useful for both nonlinear and linear least squares problems and leads to efficient algorithms, particularly for problems involving sparse matrices. The step length α_i is chosen to minimize objective function $J(\mathbf{m}_{i+1})$, with respect to α, either by line search (Fletcher, 2000), or by a direct computation. For the direct computation we insert (13) into (7), then differentiate and use (9) and (11).

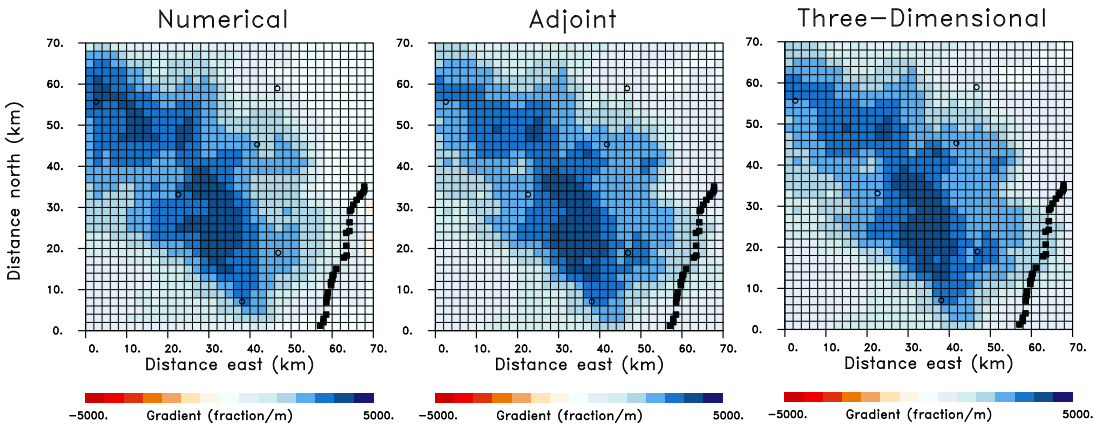

Figure 3. Data gradient components, the first term on the right-hand-side of equation (11), for source grid blocks in the top layer of the Central Valley aquifer model. The three panels correspond to three different approaches for calculating the gradient of the misfit functional. The numerical approach uses a perturbation approach to calculate the gradients and a one-dimensional elastic model. The middle panel is the gradient computed using the adjoint approach with the one-dimensional elastic model. The Three-Dimensional panel shows the gradient the results from an application of the adjoint approach with a full three-dimensional elastic model for the Tulare Basin. The units of the data gradients are $\mathrm{cm}^2/\mathrm{m}^3$ for range change data given in cm and grid block volume changes given in cubic meters.

After some algebra one finds that the partial derivative with respect to changes in α is given by

$$\frac{\partial J(\mathbf{m}_{i+1})}{\partial \alpha} = \mathbf{h}_i{}^t \nabla J(\mathbf{m}_i) + 2\alpha \mathbf{q}_i{}^t \mathbf{C}^t \mathbf{C} \mathbf{q}_i + 2\alpha\lambda \mathbf{h}_i \mathbf{R}^t \mathbf{R} \mathbf{h}_i, \tag{17}$$

where $\mathbf{q}_i$ is an additional solution to a forward problem of the form

$$\mathbf{A}\mathbf{q}_i = \mathbf{B}\mathbf{h_i}. \tag{18}$$

Setting $\partial J(\mathbf{m}_{i+1})/\partial\alpha = 0$ and solving for α gives an analytic estimate for the step length for the $i+1$-th step, based upon quantities from the previous i-th step,

$$\alpha = -\frac{\mathbf{h}_i{}^t \nabla J\left(\mathbf{m}_i\right)}{2\left[\mathbf{q}_i{}^t \mathbf{C}^t \mathbf{C} \mathbf{q}_i + \lambda \mathbf{h}_i \mathbf{R}^t \mathbf{R} \mathbf{h}_i\right]}. \tag{19}$$

Equations (10) and (11) allow us to evaluate the gradient using the equivalent of two numerical simulations, one to compute the residuals $\mathbf{e}$, and another to solve the adjoint problem (10). One additional forward solution is required to solve (18) for $\mathbf{q}_i$, giving the step length estimate α in expression (19). One can contrast the adjoint-based conjugate gradient algorithm with one that requires the computation of sensitivities. For the numerical approaches required for fully general three-dimensional models the sensitivities are calculated through numerical differencing, necessitating one numerical simulation per source grid block. In our Central Valley aquifer source model with 2 km by 2 km by 200 m cells, there are 4900 source grid blocks in total. For the actual finite-difference forward simulation our grid has a spacing of 200m along each axis for a total of 1.225 million nodes ($350\times350\times10$) and a forward run took 2.815 minutes. Thus, an entire sensitivity calculation for all 4900 source grid blocks would require roughly 230 hours of computation.

For a comparison of the conventional sensitivity-based and the adjoint-based methods of gradient calculation we consider a layered approximation to the elastic model for the region of interest. Symmetry considerations allow us to use the translational invariance of the layered model to conduct the numerical differencing for just one column of

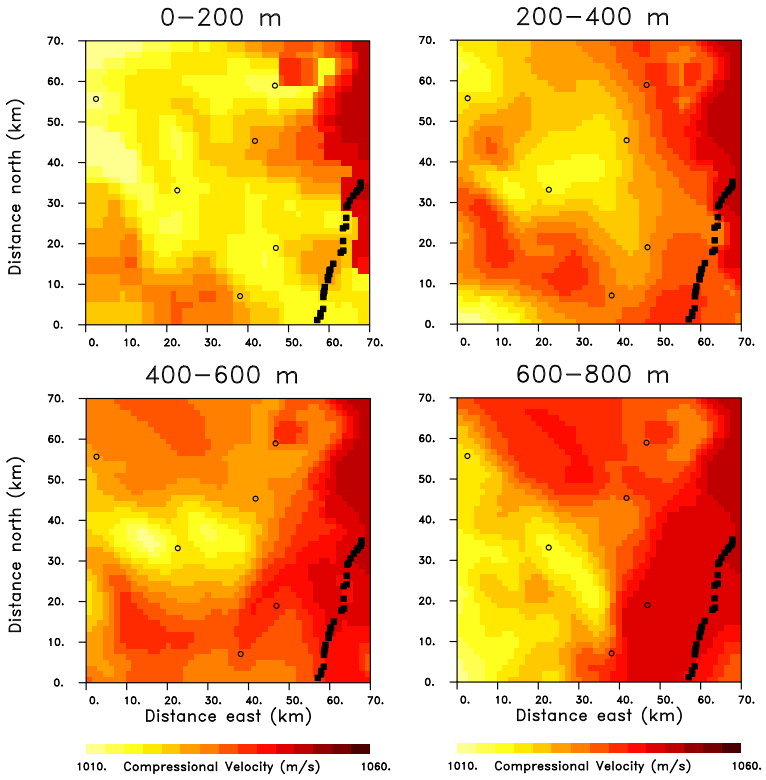

Figure 4. Laterial variations in compressional wave velocity for four depth ranges in the area under study.

grid blocks in order to compute sensitivities for the entire model. This was done using a numerical code for calculating quasi-static displacements in a layered elastic half-space (Wang et al., 2006) that we have used in previous work (Vasco et al., 2010). We plot the data gradient components based upon these sensitivities for the top layer of the model in Figure 3, along with adjoint-based gradient components from the approach detailed above. A numerical linear solver was used to find the solution to the discrete equations resulting from the finite-difference formulation. The two methods give similar data gradient estimates, and both are dominated by the pattern of range change visible in Figure 1. As indicated in equations (10) and (11), the data gradient components are just a linear mapping of the residuals.

In the Tulare Basin the actual properties in the subsurface vary spatially, and a three-dimensional model is a more accurate description of the true structure. A three-dimensional elastic model was constructed using textural variations documented in drilling logs (Faunt et al., 2010), in conjunction with two digitized sonic logs and a model of the pressure and depth dependence of sediments (Hardin & Blandford, 1989; Houlsby et al., 2005). The sediments are considered to be a mixture of a coarse, or sand-like, material and a fine, or clay-like, material. The two materials have a distinct variation with effective pressure and the sonic logs are used to determine the parameters for each material. A mixture model then provides the equivalent material properties for a given depth and a given coarse fraction of material. The spatial variation in the seismic compressional wave velocity is shown in Figure 4 for the four main layers of the model. Note that the lateral variations in velocity are not that dramatic, a roughly 5% deviation. As a result, the gradient components for the full three-dimensional model are similar to those of the layered model (Figure 3).

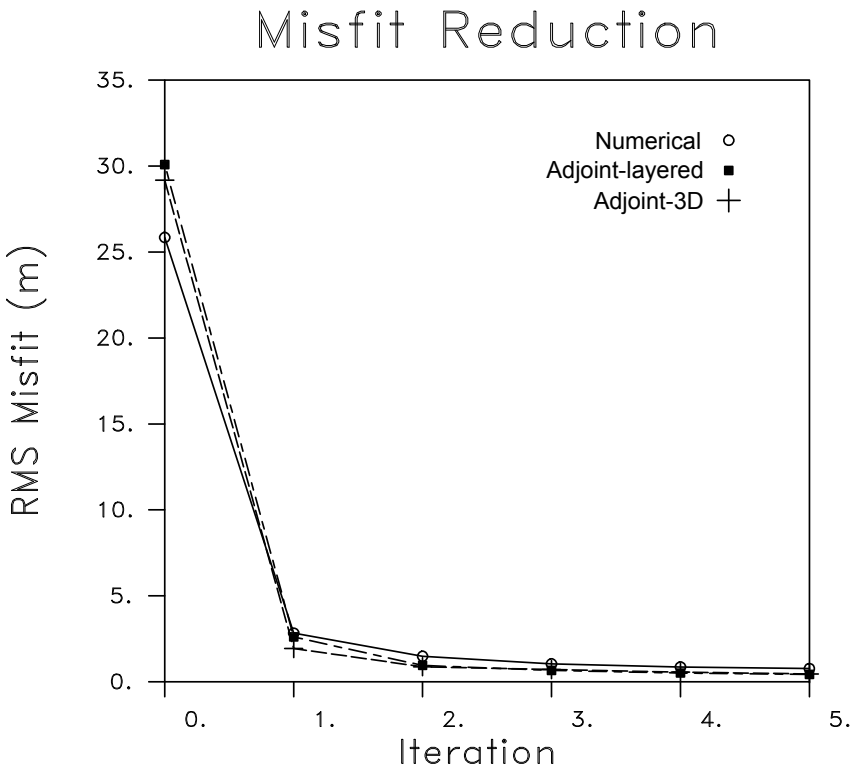

Figure 5. Misfit reduction as a function of the number of iterations taken in the conjugate gradient algorithm. The reductions for the two models using the layered elastic model are labeled 'Numerical' for the conventional sensitivity-based gradient and 'Adjoint-layered' for the adjoint-based conjugate gradient approach. The misfit reduction for the full three-dimensional adjoint-based conjugate gradient algorithm is labeled 'Adjoint-3D'.

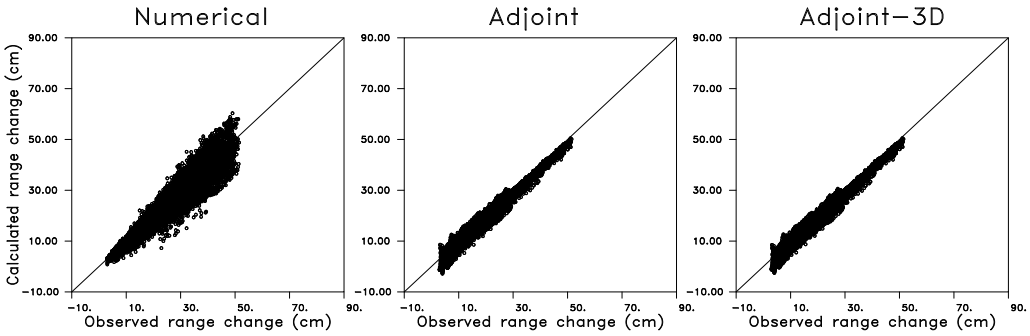

Figure 6. Fits to the observed range changes after five iterations of the three inversions schemes. (a) Observed versus calculated range changes obtained using the fifth iteration of the conjugate gradient algorithm with numerical sensitivities to calculate the range changes. (b) Comparison between the range changes calculated using the fifth iteration of the adjoint-based conjugate gradient algorithm and the layered elastic model. (c) Observed and calculated range changes for the adjoint-based conjugate gradient algorithm incorporating the full three-dimensional elastic model shown in Figure 4.

Starting from the same uniform model we initiated conjugate gradient minimization algorithms using the three approaches demonstrated in Figure 3. That is, we implemented a conjugated gradient algorithm utilizing numerical sensitivities for a layered model, an adjoint-based minimization for the layered model, and an adjoint-based three-dimensional model. The three approaches cycled through 10 iterations though they converged after the first five, as illustrated in the Figure 5. Because the layered numerical code is based upon the semi-analytic method of Wang et al. (2006), and the adjoint codes are based upon a finite-difference algorithm, the initial residuals are different for the two methods, which start from the same non-zero unit fractional volume change model. Overall, the misfit reduction for the two sets of approaches is quite similar. Hence, the use of the adjoint approach does not degrade the performance of the conjugate gradient minimization algorithm. In fact, the final misfit after 5 iterations (Figure 5) is lower for both of the adjoint solutions, approximately 50% smaller than the numerical-based inversion. This is evident in the plots of the observed range change against the calculated range change in Figure 6. Because the data, regularization, and conjugate gradient algorithm are the same for the numerical and adjoint approaches, the differences in the final fits are most likely due to the small differences in the gradients. We found that the largest residuals were near the edges of the model where the cells are not constrained by data outside the boundaries of the model and the well regularization still allows for significant volume change. These large residuals were removed by adding an additional model norm constraint. Note that the scatter in the residuals for the three solutions is larger than the formal errors in the InSAR data, which are of the order of 1 centimeter, suggesting that the modeling errors dominate the misfit. In particular, the large 2 km (x) by 2 km (y) by 200 m (z) grid blocks mean that the model cannot represent smaller scale variations found in the data. A finer scale model would reduce such misfit but would considerably increase the computational requirements.

The volume changes in the top three layers of the models are plotted in Figure 7 in terms of the percentage of grid block volume. The patterns of volume change are similar for the three approaches and change systematically with depth, following the pattern of well distributions plotted in Figure 2. The estimated total volume loss in the aquifer during the two year period from January 2016 to January 2018 was 2.17 cubic kilometers/year. This value in of the same order as the loss of water volume estimates from the

analysis of GRACE satellite gravity data, 3.1 km^3/year, which covered the entire Central Valley and a substantial portion of the California drought (Richley et al., 2015). The estimated volume changes are in agreement with recent work (Vasco et al., 2019) and thus, as shown in that paper, are compatible with known well extraction rates and calculated crop water requirements. The two year period considered here encompasses one year at the and of the recent drought (2016) and a very wet year (2017). The inclusion of the three-dimensional elastic model changed some of the details from the layered solution, particularly the amplitudes in certain areas. However, the overall pattern did not change significantly.

4 Discussion and Conclusions

The adjoint methods that have proven valuable in various areas of geophysics, such as seismic waveform inversion (Tarantola, 2005; Fichtner, 2010), are also useful in the inversion of quasi-static geodetic data for distributed source models. For a formulation in terms of displacements, one step in an iterative model updating approach simply requires the computational equivalent of three numerical simulations: one to compute the residuals, one to solve the adjoint problem for the gradient, and a final one to calculate the step length. The application to Interferometric Synthetic Aperture Radar data illustrates that the approach is practical for problems involving more than 1 million grid points. In fact, the adjoint-based inversion accounting for the full three-dimensional structure results in a somewhat better fit to the InSAR observations than does a conventional seisntivity-based approach (Figures 5 and 6). The final models plotted in Figure 7 all share the same general features and similar variations in depth. The depth variations for all of the models reflects the changes in the well configurations for each depth interval. Thus, even though the surface deformation looks very different from the distribution of wells at depth, the results indicate that a source model with changes near known wells can indeed satisfy the InSAR observations. There are differences in the detailed distribution of volume change in the three models, due to the small deviations in the solution to to forward problem, such as the numerical convergence criteria and boundary conditions that lead to variations in the gradients (Figure 3). These differences can be amplified due to the inherent instability of the inverse problem, even though regularization terms are included.

The iterative approach for solving the inverse problem allows for increased efficiency in both computational time and memory requirements. In that sense, it shares characteristics with iterative linear solvers such as the least squares QR algorithm (LSQR) (Paige & Saunders, 1982) which can be interpreted as the application of a conjugate gradient method. Conjugate gradient metods are particularly well suited for problems that are sparse in some sense (Press et al., 1992), such as those defined in terms of discretized partial differential equations. The application presented here involves one of the simpler cases, a linear elastic medium, and a formulation solely in terms of displacements. Other formulations, such as a specification in terms of velocity and stress, can also be treated with the appropriate scalings (Kaderli et al., 2018). The adjoint-based techniques have been applied to general coupled simulators, so the approaches should be applicable to poroelastic, viscoelastic, and general nonlinear deformation. This may require reformulations, such as a transformation into the frequency domain, in order to map the convolutions that occur in time-domain poroelastic and viscoelastic problems into multiplications. Or it may require seperating out the anelastic effects from the elastic strain for viscoelastic and poroelastic problems (D'Agostino et al., 2018). A general nonlinear deformation might be broken up into a sequence of linearized step, with the adjoint-based methodology applied to each increment. There are many areas where large-scale models of deformation sources could be useful, including geothermal activities, carbon sequestration, reservoir injection and production, groundwater management, as well as in monitoring volcanic processes.

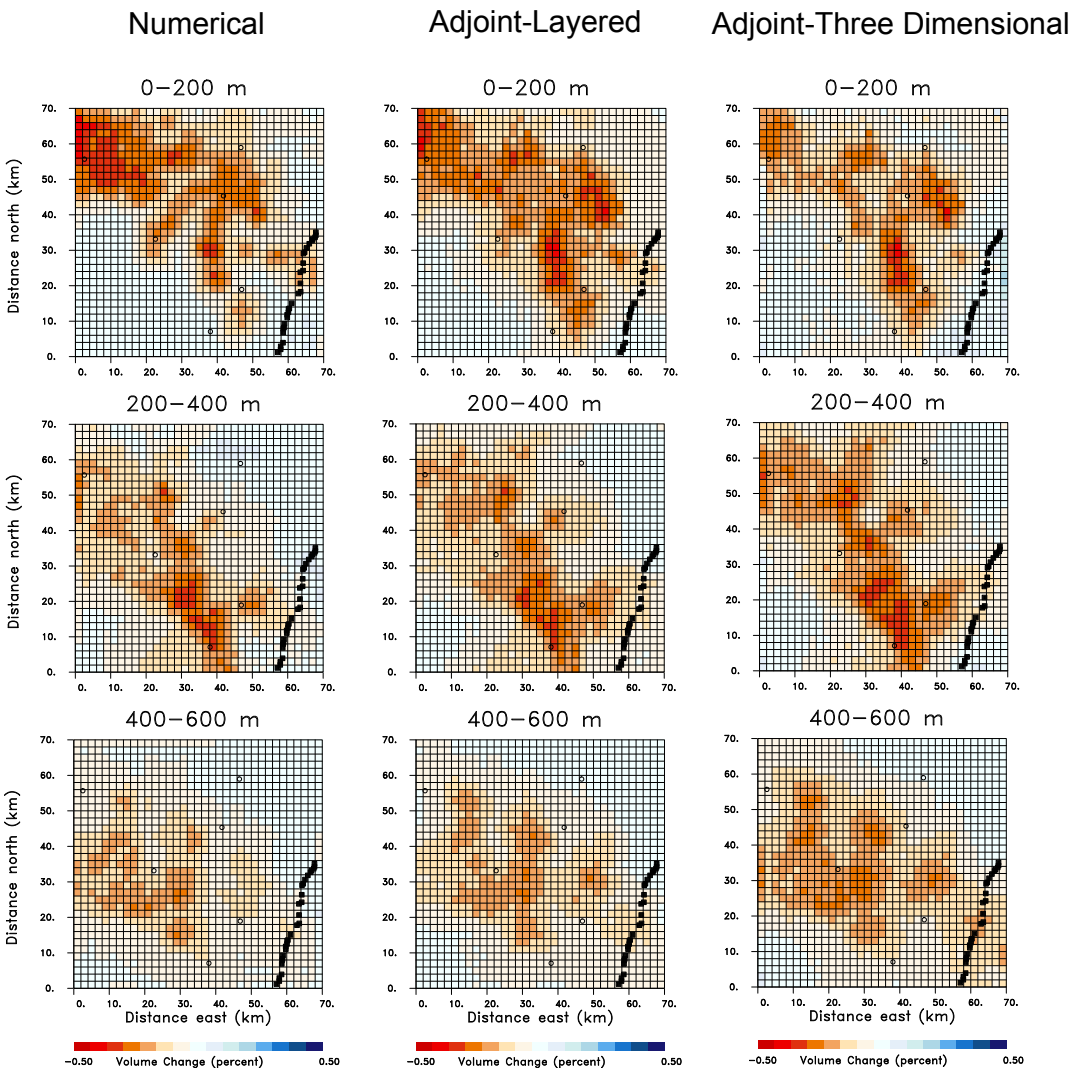

Figure 7. The results from three distinct inversions of the InSAR range change data in Figure 1. The panels designated as 'Numerical' are the result of a conjugate gradient algorithm utilizing a layered elastic model and symmetry in order to calculate the sensitivities used in the gradient computatation. The panels in the column labeled 'Adjoint-Layered' show the results from an inversion that used an equivalent layered model but employing the adjoint-based approach described above for the inversion. The right-most panels, under the label 'Adjoint-Three dimensional' utilized the full three-dimensional model shown in Figure 4, in conjunction with the adjoint-based gradients.

Acknowledgments
The development of the technique was supported by the U.S. Department of Energy, Office of Science, Office of Basic Energy Sciences, Chemical Sciences, Geosciences, and Biosciences Division under contract number DE-AC02-05-CH11231 and Chevron. The application to the InSAR observations in California's Central Valley was supported by a grant from the California Energy Commission. The InSAR observations used in this project are available from the Zenodo repository via the pathway http://doi.org/10.5281/zenodo.4420364. The entire citation for the data set is:

Donald W. Vasco, J. Torquil Smith. (2021). InSAR data from 2016 to 2018 for the Tulare Basin in California's Central Valley. Zenodo. http://doi.org/10.5281/zenodo.4420364.

The estimates of line-of-sight displacement were obtained from the European Space Agency's Sentinel 1a/b satellite pair based upon a processing stream described in (Farr & Liu, 2015).

References

Chang, W.-L., Smith, R. B., Wicks, C., Farrell, J. M., & Puskas, C. M. (2007). Accelerated uplift and magmatic intrusion of the yellowstone caldera, 2004 to 2006. *Science*, *318*, 952-956.

D'Agostino, N., Silverii, F., Amoroso, O., Corvertito, V., Fiorillo, F., Ventafridda, G., & Zollo, A. (2018). Crustal deformation and seismicity modululated by groundwater recharge of karst aquifers. *Geophysical Research Letters*, *45*, 12,253-12,262.

Farr, T. G., & Liu, Z. (2015). Monitoring subsidence associated with groundwater dynamics in the central valley of califonia using interferometric radar. In *Remote sensing of the terrestrial water cycle, geophysical monograph 206.* V. Lakshmi (Ed.), American Geophysical Union, John Wiley and Sons.

Faunt, C. C., Belitz, K., & Hanson, R. T. (2010). Development of a three-dimensional model of sedimentary texture in valley-fill deposits of central valley, california, usa. *Hydrogeology Journal*, *18*, 625-649.

Ferretti, A. (2014). *Satellite insar data: Reservoir monitoring from space.* European Association of Geoscientists and Engineers.

Fichtner, A. (2010). *Full seismic waveform modelling and inversion.* Heidelberg: Springer.

Fielding, E. J., Blom, R. G., & Goldstein, R. M. (1998). Rapid subsidence over oil fields measured by sar interferometry. *Geophysical Research Letters*, *25*, 3215-3218.

Fletcher, R. (2000). *Practical methods of optimization.* Cornwall: John Wiley and Sons.

Galloway, D. L., Hudnut, K. W., Ingebritsen, S. E., Phillips, S. P., Peltzer, G., Rogez, F., & Rosen, P. A. (1998). Detection of aquifer system compaction and land subsidence using interferometric synthetic aperture radar, antelope valley, mojave desert, california. *Water Resources Research*, *34*, 2573-2585.

Gwinner, J., & Stephan, E. P. (2018). *Advanced boundary element methods.* Cham, Switzerland: Springer.

Hardin, B. O., & Blandford, G. E. (1989). Elasticity of particulate materials. *Journal of Geotechnical Engineering*, *115*, 788-805. doi: 10.1061/(ASCE)0733-9410(1989)115:6(788)

Hatchell, P., & Bourne, S. (2005). Rocks under strain: Strain induced time-lapse timeshifts are observed for depleting reservoirs. *The Leading Edge*, *24*, 1222-1225.

Hattel, J. H., & Hansen, P. N. (1995). A control volume-based finite difference method for solving the equilibrium equations inn terms of displacements. *Appl. Math. Modelling*, *19*, 210-243.

Hesse, M. A., & Stadler, G. (2014). Joint inversion in coupled quasi-static poroelasticity. *Journal of Geophysical Research*, *119*, 1425-1445.

Hodgson, N., MacBeth, C., Duranti, L., Rickett, J., & Nihei, K. (2007). Inverting for reservoir pressure changes using time-lapse time strain: Application to the genesis field, gulf of mexico. *The Leading Edge*, *26*, 649-652.

Houlsby, G. T., Amorosi, A., & Rojas, E. (2005). Elastic moduli of soils dependent on pressure: a hyperelastic formulation. *Geotechnique*, *55*, 383-392.

Iglesias, M. A., & McLaughlin, D. (2012). Data inversion in coupled sub-surface flow and geomechanical models. *Inverse Problems*, *28*.

Jacquard, P., & Jain, C. (1965). Permeability distribution from field pressure data. *Society of Petroleum Engineering Journal*, *5*, 281-294.

Kaderli, J., McChesney, M. D., & Minkoff, S. E. (2018). A self-adjoint velocity-stress full-waveform inversion approach to microseismic source estimation. *Geophysics*, *83*, R413-R427.

Liu, Z., Liu, P.-W., Massoud, E., Farr, T. G., Lundgren, P., & Famiglietti, J. S. (2019). Monitoring groundwater change in california's central valley using

sentinel-1 and grace observations. *Geosciences*, *9*, 1-20.

Menke, W. (2018). *Geophysical data analysis: Discrete inverse theory*. London: Academic Press.

Moore, J. D. P., Yu, H., Tang, C.-H., Wang, T., Barbot, S., Peng, D., ... Shibazaki, B. (2017). Imaging the distribution of transient viscosity after the 2016 m_w 7.1 kumamoto earthquake. *Science*, *356*, 163-167.

Murray, K. D., & Lohman, R. B. (2018). Short-lived pause in central california subsidence after heavy winter precipitation of 2017. *Science Advances*, *4*, 1-8.

Neely, W. R., Borsa, A. A., Burney, J. A., Levy, S. F., M. C., & Sneed, M. (2020). Characterization of groundwater recharge and flow in california's san joaquin valley from insar-observed surface deformation. *Water Resources Research*, *57*, 1-20.

Paige, C. C., & Saunders, M. A. (1982). Lsqr: An algorithm for sparse linear equations and sparse linear systems. *ACM Trans. Math. Software*, *8*, 195-209.

Phillips, T. N., & Rose, M. E. (1986). A finite difference scheme for the equilibrium equations of elastic bodies. *SIAM J. Sci. Stat. Comput.*, *7*, 288-300.

Plessix, R. E. (2006). A review of the adjoint-state method for computing the gradient of a functional with geophysical applications. *Geophysical Journal International*, *167*, 495-503.

Press, W. H., Teukolsky, S. A., Vetterling, W. T., & Flannery, B. P. (1992). *Numerical recipes*. Cambridge: Cambridge University Press.

Richley, A. S., Thomas, B. F., Lo, M.-H., Reager, J. T., Famiglietti, J. A., Voss, K., ... Rodell, M. (2015). Quantifying renewable groundwater stress with grace,. *Water Resources Research*, *51*, 5217-5238.

Stakgold, I. (1979). *Green's functions and boundary value problems*. New York: John Wiley and Sons.

Tarantola, A. (2005). *Inverse problem theory and methods for model parameter estimation*. Philadelphia: SIAM.

Vasco, D. W., Farr, T. G., Jeanne, P., Doughty, C., & Nico, P. (2019). Satellite-based monitoring of groundwater depletion in california's central valley. *Scientific Reports*, *9*, 1-14. doi: https://doi.org/10.1038/s41598-019-52371-7

Vasco, D. W., Harness, P., Pride, S., & Hoversten, M. (2017). Estimating fluid-induced stress changes from observed deformation. *Geophysical Journal International*, *208*, 1623-1642.

Vasco, D. W., & Mali, G. (2021). On the use of adjoints in the inversion of observed quasi-static deformation. *Geophysical Journal International*, *224*, 896-908.

Vasco, D. W., Rucci, A., Ferretti, A., Novali, F., Bissell, R., Ringrose, P., ... Wright, I. (2010). Satellite-based measurements of surface deformation reveal flow flow associated with the geological storage of carbon dioxide. *Geophysical Research Letters*, *37*, 1-5. doi: 10.1029/2009GL041544

Wang, R., Lorenzo-Martin, F., & Roth, F. (2006). Psgrn/pscmp–a new code for calculating co- and post-seismic deformation, geoid and gravity changes based on the viscoelastic-gravitational dislocation theory. *Computers in Geoscience*, *32*, 527-541.